UDC 621.43.004.62

J. L. PEREZ RUIZ, I. I. LOBODA

Instituto Politecnoco Nacional,
Escuela Superior de Ingenieria Mecanica y Electrica, Mexico

A FLEXIBLE FAULT CLASSIFICATION FOR GAS TURBINE DIAGNOSIS

Diagnostic algorithms that use gas path measurements and models are capable to diagnose not only different faults of the gas path itself but also malfunctions of measurement and control systems. Since the variety of gas turbine fault conditions is great, they are joined in a limited number of classes. Different principles to create these classes are known and there are many fault classifications in practice. In an investigation stage, it is difficult to predict what classification will then be applied in a real monitoring system therefore the investigators usually experiment with different fault types and fault numbers. The present paper proposes the approach that allows simple creating multiple classification variations including complex and realistic fault classes. This approach also permits easy changing between the variations and the pattern recognition techniques applied for each variation. As a result of application of each technique to each classification, probability of correct diagnostic decisions and execution time are determined. They are criteria of diagnosis efficiency. In this way, the approach allows studying the influence of fault classification on diagnosis efficiency. The paper performs such a study for a power plant for natural gas pipelines. Twelve classification variations are analyzed with the use of three recognition techniques: Multi-Layer Perceptron, Radial Basis Network and Probabilistic Neural Network. Additionally, a new boundary for fault severity is proposed and investigated by comparing three boundary options.

Key words: *gas turbine diagnosis, pattern recognition, flexible fault classification, fault severity boundary.*

Introduction

In modern gas turbine health monitoring systems, diagnostic algorithms based on gas path analysis may be considered as principal. They analyze gas path measured variables and are capable of identifying different faults and degradation mechanisms of gas turbine components (e.g. compressor, turbine, and combustor) as well as malfunctions of the measurement system itself (sensor errors).

The fault identification algorithms widely use the pattern recognition theory and, in the last three decades, the use of many recognition techniques has been reported: first of all, Artificial Neural Networks [1], and also Bayesian Approach [2], Support Vector Machines [3], and nonparametric methods [4]. The necessary fault classification is mainly constructed by using a gas path mathematical model. It relates gas path monitored variables with special fault parameters that shift a little the performance maps of engine components (compressors, turbines, burner and others). The maps of each component can be shifted in different directions therefore the model is capable to simulate all possible engine faults and degradation mechanisms.

Fault classes of two types are generally created using the model. A class of single faults of varying severity is formed by changing one fault parameter while a class of multiple faults is formed by independent varying of two or more fault parameters. The classification structure (faulted engine, type of classes, and their number) depends on many factors. Even for the same engine, the classification can vary a lot. Investigating diagnostic algorithms, it is difficult to predict what classification variation will be finally used in a real monitoring system. For this reason, some more probable classification variations are usually analyzed.

In our previous studies [2, 4, 5], only two rigid variations were considered: a classification with only single fault classes and a classification with only multiple fault classes formed by two fault parameters.

The purpose of the present work is to investigate how the classification influences gas turbine diagnostic accuracy. To this end, a flexible fault classification is proposed. The procedure that realizes this classification allows easy creating any new classification variation that can be more complex and more realistic then the classifications previously analyzed. Twelve variations have been prepared for examining in this paper.

The procedure also permits simple choosing the variation to be currently examined. For this fault classification, many fault patterns are generated and diagnosed by one of three neural networks: Multi-Layer Perceptron (MLP), Radial Basis Network (RBN) and Probabilistic Neural Network (PNN). For each network, a probability of correct diagnosis is finally determined to be criteria of diagnostic accuracy. Using these criteria and execution time as an additional criterion, the networks are compared within each classification variation.

Such an analysis allows better choosing the best diagnostic technique. An average probability provided by the three networks allows comparison of classification variation. An optimal classification structure can be found as a tradeoff between this probability and the width of coverage of possible component faults.

The paper also introduces and studies a new boundary for fault severity. With this boundary, the fault class description becomes more realistic thus providing more accurate diagnosis.

1. Gas turbine models

1.1. Nonlinear thermodynamic model

This thermodynamic model computes a (m×1)-vector $\vec{Y}$ of gas path monitored variables as a function of a vector $\vec{U}$ of steady state operational conditions (control variables and ambient conditions) as well as a (r×1)-vector $\vec{\Theta}$ of fault parameters, which can also be named health parameters or correction factors depending on addressing problems. Given the above explanation, the thermodynamic model has the following structure:

$$\vec{Y} = F\left(\vec{U}, \vec{\Theta}\right). \qquad (1)$$

There are various types of gas turbine deterioration and faults such as fouling, tip rubs, seal wear, erosion, and foreign object damage. Since such real defects occur rarely during maintenance, the thermodynamic model is a unique technique to create necessary class descriptions. To take into account the component performance changes induced by real gradual deterioration mechanisms and abrupt faults, the fault parameters $\vec{\Theta}$ that shift a little the components' maps as shown in Fig.1.

Mathematically, the model is a system of nonlinear algebraic equations reflecting mass, heat, and energy balance for all components operating under stationary conditions.

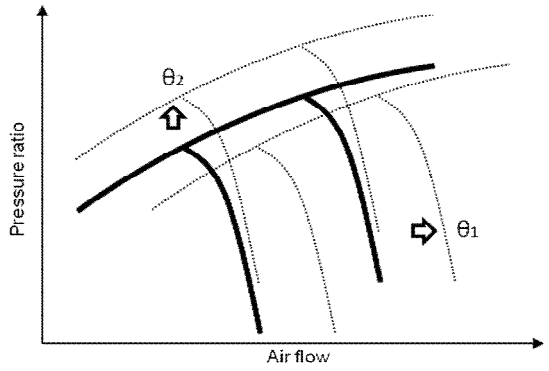

Fig. 1. Compressor map shifting by the fault parameters

The thermodynamic model for steady states has wide applications in gas turbine diagnostics. First, as shown before and in more detail in [5], this model is used to describe particular faults or complete fault classification. Second, the thermodynamic model is an integral part of numerous diagnostic algorithms based on system identification such as described in [6]. Third, this nonlinear model allows computing simpler models, like a linear model used in [7] and in the present paper to create flexible fault classifications.

1.2. Linear static model

The linear static model presents linearization of nonlinear dependency $\vec{Y} = f_2\left(\vec{\Theta}\right)$ between gas path variables and fault parameters determined for a fixed operating condition $\vec{U}$. The model is given by a vectorial expression:

$$\delta\vec{Y} = H\delta\vec{\Theta}. \qquad (2)$$

It connects a vector $\delta\vec{\Theta}$ of small relative changes of the fault parameters with a vector $\delta\vec{Y}$ of the corresponding relative deviations of the monitored variables by a matrix H of influence coefficients (influence matrix).

Since linearization errors are not too great, about some per cent, the linear model can be successfully applied for fault simulation at any fixed operating point. However, when it is used for estimating fault parameters by system identification methods like in study [6,8], estimation errors can be significant. Given the simplicity of the linear model and its utility for analytical analysis of complex diagnostic issues, this model will remain important in gas turbine diagnostics.

2. Methodology for gas turbine diagnosis

2.1. Deviations

By direct analysis of the variables themselves it is difficult to discriminate performance degradation effects from great changes due to different operating modes. To draw useful diagnostic information from raw recorded data, a total gas turbine diagnostic process usually includes a preliminary procedure of computing deviations. The deviations are defined as differences between measured and engine baseline values. As the baseline depends on an engine operating condition, it can be written as function $\vec{Y}_0(\vec{U})$ usually called a baseline function. With this model the deviations for each monitored variables $Y_{i,i=1,m}$ is computed in a relative form:

$$\delta Y_i^* = \frac{Y_i^* - Y_{0i}\left(\vec{U}\right)}{Y_{0i}\left(\vec{U}\right)}, \qquad (3)$$

where Y_i^* denotes a measured value.

2.2. Diagnostic space

As mentioned before, models are used in gas turbine diagnostics to describe engine performance degradation and faults and the deviations are employed to reveal the degradation influence. These deviations are written in relative form and normalized so as to facilitate simulating faults and their subsequent recognition. At a steady state, the deviation is defined for *i*-th measured variable as:

$$Z_i = \frac{Y_i\left(\vec{U},\vec{\Theta}_0+\delta\vec{\Theta}\right)-Y_{0i}\left(\vec{U},\vec{\Theta}_0\right)}{Y_{0i}\left(\vec{U},\ \vec{\Theta}_0\right)\sigma_{Yi}}, \qquad (4)$$

where σ_{Yi} is the amplitude of possible random fluctuations in the original deviation δY_i^*. To take into account possible measurement errors, the vector $\vec{\varepsilon}$ of random variables distributed within the interval (-1,1) is added. A resultant vector

$$\vec{Z}^* = \left(\vec{Z}+\vec{\varepsilon}\right) \qquad (5)$$

corresponds to the deviations that are calculated in practice for actual measurements.

2.3. Principles for developing classification

Engine faults vary considerably. Hence, for the purposes of engine diagnostics this variety has to be broken down into a limited number of classes. In the pattern recognition theory, it is often supposed that an object state D can belong only to one of q present classes

$$D_1,\ D_2,\ldots,D_q. \qquad (6)$$

Consequently

$$\sum_{j=1}^{q} D_j = 1 \quad \text{and} \quad P_{j\neq l}(D_j / D_l) = 0. \qquad (7)$$

We accept this hypothesis for a gas turbine fault classification.

Fault classifications can contain two different types of fault classes: singular or multiple classes. The first type works with only one fault parameter while the second one is formed by independent changes of two or more fault parameters in order to represent more complex faults in gas turbines.

For each class, singular or multiple, numerous patterns $\vec{Z}$ are generated according to expression (4) setting the necessary quantities $\delta\Theta_j$ and ε_i by the uniform and Gaussian distributions accordingly. A typical number of patterns per class is 1000. A totality $\mathbf{Z_L}$ of all classification's patterns is employed to train the used neural network and is therefore called a learning set.

2.4. Recognition decision making

A nomenclature of possible diagnosis $d_1,\ d_2,\ldots,d_q$ made by a recognition technique (neural network within the present paper) corresponds to the accepted classification (6). To make a diagnosis d, a criterion $R_j = R(\vec{Z}^*, D_j)$ specific for each technique is introduced as a measure of membership of a current pattern $\vec{Z}^*$ in class D_j. To determine the functions $R_j = R(\vec{Z}^*, D_j)$, a learning set Z_L is used. After calculating all values R_j, $j = 1,q$, a decision rule

$$d = d_l \ \text{ if } \ R_l = \max\left(R_1, R_2,\ldots,\ R_q\right) \qquad (8)$$

is applied.

2.5. Recognition accuracy

To verify a recognition technique determined with the help of the learning set, one more set is required. The necessary set $\mathbf{Z_V}$, called a validation set, is created in the same way as the set $\mathbf{Z_L}$. The only difference is that other series of random numbers is generated to simulate fault severity and errors in the deviations.

Every pattern in the validation set belongs to a known class. Comparing this class D_j with the diagnosis d_l, we can compute probabilities $Pd_{lj} = P\left(d_l / D_j\right)$ and compose a confusion matrix (Table 1). Its diagonal elements Pd_{ll} form a vector $\vec{P}$ of true diagnosis probabilities that are indices of classes' distinguishability. Mean number of these elements – scalar $\overline{P}$ – characterizes total engine diagnosability. No diagonal elements are wrong diagnosis probabilities. They help to identify the causes of bad class distinguishability. For 1000 patterns per class, the computational precision of the mean probability $\overline{P}$ is approximately ±0.01. In order to enhance the precision, each calculation of $\overline{P}$ is repeated in the present study 100 times, each time with new series of random numbers. The 100 corresponding random values of $\overline{P}$ are averaged, resulting in a probability P_{av} with higher precision of ±0.001.

Table 1

Confusion matrix

Diagnosis	Classes			
	D_1	D_2	…	D_q
d_1	Pd_{11}	Pd_{12}	…	Pd_{1q}
d_2	Pd_{21}	Pd_{22}	…	Pd_{2q}
…	…	…	…	…
d_q	Pd_{q1}	Pd_{q2}	…	Pd_{qq}

3. Pattern recognition techniques

Three different artificial neural networks described below have been chosen in the present study for gas turbine fault recognition.

3.1. Multi-Layer Perceptron (MLP)

The MLP is a feedforward artificial neural network model that maps sets of input data onto a set of appropriate outputs. It consists of multiple layers of nodes in a directed graph, with each layer fully connected to the next one. Except for the input nodes, each node is a neuron with a nonlinear activation function (Fig. 2). When the perceptron is applied to a classification problem, each output *k* gives a closeness measure between the analyzed input pattern $\vec{Z}$ and a class D_k.

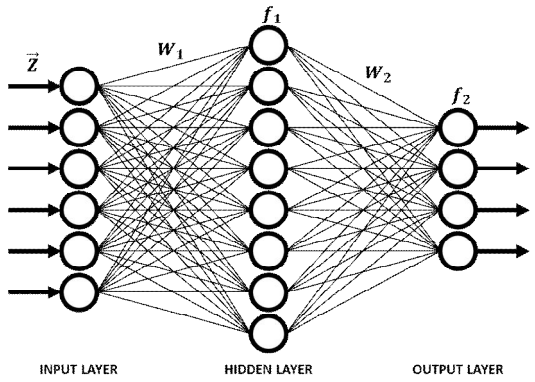

Fig. 2. Typical MLP structure

During the learning, unknown weight coefficients and biases are determined by a back-propagation algorithm, in which a network output error is propagated backwards to correct these unknown quantities. They are corrected in the direction that reduces the error unless a global error minimum is reached. The back-propagation algorithm needs differentiable transfer functions and they usually are of a sigmoid or linear type. MLP is a modification of the standard linear perceptron and can distinguish data that are not linearly separable

3.2. Radial Basis Network (RBN)

A RBN is an artificial neural network that uses radial basis functions as activation functions. The output of the network is a linear combination of radial basis functions of the inputs and neuron parameters. A radial basis neuron operates as follows. Neuron's weight coefficients form a weight vector that is one of learning patterns. First, a distance between the weight vector and an input vector $\vec{Z}$ is computed. This distance is then divided by a bias b resulting in an input n to a radial basis transfer function (RBF). The RBF finally computes a neuron's output according to an expression $a = e^{-n^2}$. When the distance is 0, this function has a maximum value $a = 1$. The function decreases when the distance increases. The bias b allows changing an action area (window) of the neuron and is called spread. The output layer of the RBN works similarly to a usual perceptron output layer with a linear transfer function.

3.3. Probabilistic Neural Network

A probabilistic network, specific type of radial basis networks, is specially intended for classification problems. It consists of three layers. The hidden layer is formed and operates just like the same layer of the RBN algorithm. It is built from learning patterns united in a matrix W_1. Each learning pattern $\vec{w}_{1j}$ specifies a center of the RBN of one hidden neuron. A Euclidean distance L_j between the function center $\vec{w}_{1j}$ and the input pattern $\vec{Z}$ is firstly computed. The distance L_j divided by the spread *b* is a hidden neuron input. A radial basis function f_{1j} then calculates a neuron output $a_{1j} = f_{1j} = e^{-L_j^2/b^2}$. The closer the input vector is situated to the neuron center, the greater the neuron output will be. Thus, elements of a vector $\vec{a}_1$ indicate how close the input pattern is to the learning patterns.

The output or classification layer differs from the RBN output layer. Each classification neuron corresponds to one of the analyzed classes. An input of the classification neuron, which is interpreted as a probability of this class, is computed as a sum of the signals a_{1j} related with the learning patterns of the same class. In other words, each hidden neuron is connected with only one classification neuron and connection weights are equal to one. To realize such a connection, a matrix W_2 is composed in a particular way from zero and one elements and a product $W_2\vec{a}_1$ is computed. It is an input vector for the classification layer and consists of probabilities of all considered classes. Finally, the classification layer transfer function f_2 produces a 1 corresponding to the largest probability, and 0's for the other network outputs. Thus, the PNN classifies the input vector $\vec{Z}$ into a specific class on the basis of a probability measure.

4. Calculation conditions

The approach and three neural networks described above were applied for diagnosing a turboshaft stationary power plant with a free turbine intended for driving a centrifugal compressor in natural gas pipelines. Five components of the engine are diagnosed: inlet device, axial compressor, combustion chamber, compressor turbine and

power turbine. An engine operating point is given by a constant compressor rotational speed 10700 rpm and standard atmospheric conditions. The six gas path variables of Table 2 corresponding to an engine standard measurement system are available for monitoring. To simulate gas path and measurement system faults, the eighteen fault parameters from Table 3 are involved.

Table 2

Monitored variables

Number	Variable*	Symbol
1	Compressor pressure	P_c
2	Turbine pressure	P_t
3	Compressor temperature	T_c
4	Turbine temperature	T_t
5	Power turbine temperature	T_{pt}
6	Fuel flow	G_f

* component pressures and temperatures correspond to a component discharge section

Table 3

Fault parameters

Number	Fault parameter	Symbol
1	Compressor air flow	δG_c
2	Compressor efficiency	$\delta \eta_c$
3	Turbine gas flow	δG_t
4	Turbine efficiency	$\delta \eta_t$
5	Power turbine gas flow	δG_{pt}
6	Power turbine efficiency	$\delta \eta_{pt}$
7	Combustion chamber pressure recovery factor	$\delta \sigma_{cc}$
8	Combustion efficiency	$\delta \eta_{cc}$
9	Inlet pressure loses factor	$\delta \sigma_{in}$
10	Compressor pressure	δP_c
11	Turbine pressure	δP_t
12	Compressor temperature	δT_c
13	Turbine temperature	δT_t
14	Power turbine temperature	δT_{pt}
15	Fuel flow	δG_f
16	Inlet pressure	δP_{in}
17	Inlet temperature	δT_{in}
18	High pressure turbine speed	δn_{hp}

On the basis of the fault parameters specified in Table 3, the next section introduces various fault classification variations.

5. Fault classification variations

With the intention of studying the influence of the fault classification structure on final diagnostic accuracy, twelve fault variations are introduced. These variations contain different class quantities, fault parameters, fault development directions (positive or negative) and engine components. These variations are specified in Table 4 and additionally briefly described below.

– Variation 1: It has nine singular classes formed by gas path parameters whose changes are negative;

– Variation 2: It is formed by four multiple classes with two gas path parameters per class and grouped by an engine component: compressor, turbine, power turbine and combustion chamber (Fig. 3);

– Variation 3: The combination of variation 1 and three singular classes with positive direction of a fault parameter (turbine and power turbine air flow parameters and combustion chamber pressure ratio) to simulate burns in hot parts;

– Variation 4: The combination of variation 2 + three multiple classes formed by turbine and power turbine air flow parameters, combustion chamber pressure ratio and their respective efficiencies (negative direction);

– Variation 5: It contains six singular classes of sensor faults in $\vec{Y}$. Each of them has positive and negative directions of fault;

– Variation 6: The combination of variations 3 and 5 resulting in eighteen singular classes to simulate gas path faults and sensor errors;

– Variation 7: Formed by seven multiple classes of variation 4 and six singular classes (sensor faults) with double limits;

– Variation 8: It has the six sensor faults in $\vec{Y}$ and three singular classes of sensor faults in $\vec{U}$;

– Variation 9: Formed by three multiple classes (turbine and power turbine air flow parameters, combustion chamber pressure ratio and their respective efficiencies) and one multiple class of faults in compressor;

– Variation 10: It contains nine singular classes: three singular classes with double direction of fault (turbine and power turbine air flow parameters and combustion chamber pressure ratio), four efficiencies for all components, one for the compressor air flow and another one for the inlet pressure loses factor;

– Variation 11: In this variation, each class is created by four fault parameters. It is formed by the combination of air flow parameters (with the exception of the combustion chamber pressure ratio) and efficiencies. The first three classes are formed by combining the turbine, the power turbine and the combustion chamber with the compressor, the fourth and the fifth - by combining the power turbine and the combustion chamber with the turbine. The last class is formed as the combination of the power turbine and the combustion chamber (Fig. 4);

– Variation 12: It is practically the same as variation 11, but, in this case all the classes have negative directions to simulate gas path faults.

For each classification variation, fault diagnosis was performed by with three neural networks: Multi-Layer Perceptron, Radial Basis Network and Probabilistic Neural Network and the probability P_{av} and execution time were determined for each network. Table 5 shows all the results. All the computation was performed in a Dell Inspiron One Desktop: Intel Pentium

G2020T processor, 2.5 GHz, and 4 GB of RAM.

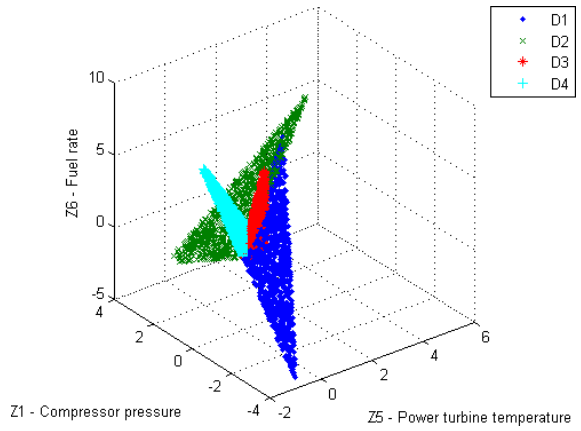

Fig. 3. Classification variation 2: four multiple classes with two fault parameters

Analyzing the probabilities, one can state that the differences between the networks within the same classification variation are not great (excepting variation 6), about 0.015 (1.5%), while the difference between the variations can reach the value 0.10. Thus, these results reaffirm once more the conclusion drawn in [9] that many recognition techniques may yield the same gas turbine diagnosis accuracy.

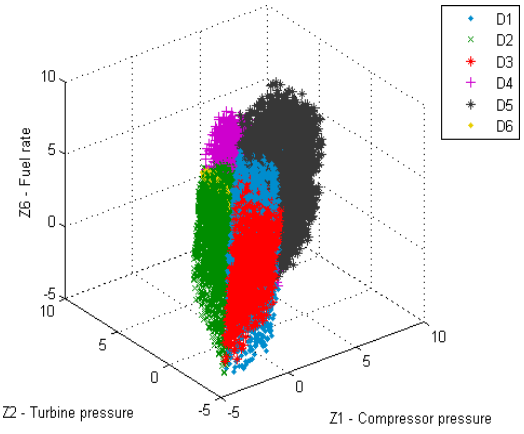

Fig. 4. Classification variation 11: six multiple classes with four fault parameters

The execution time includes 100 cycles of calculation of the mean probability $\overline{P}$. Each cycle consists of a learning stage with thousands diagnosis cycles of a validation stage at which the probability $\overline{P}$ is computed. In Table 5, we can see that this total time is by far smaller for the PNN for all classifications. This is explained by the fact that this network does not need a learning stage. Thus, the PNN seems to be the simplest network to tailor for gas turbine diagnosis.

Table 4

Variations of classification and their fault class formation

VARIATION	FAULT CLASSES																	
	1	2	3	4	5	6	7	8	9	10	11	12	13	14	15	16	17	18
Variation 1	$-\delta G_c$	$-\delta\eta_c$	$-\delta G_t$	$-\delta\eta_t$	$-\delta G_{pt}$	$-\delta\eta_{pt}$	$-\delta\sigma_{cc}$	$-\delta\eta_{cc}$	$-\delta\sigma_{in}$									
Variation 2	$-\delta G_c$ - $\delta\eta_c$	$-\delta G_t$ $-\delta\eta_t$	$-\delta G_{pt}$ $-\delta\eta_{pt}$	$-\delta\sigma_{cc}$ $-\delta\eta_{cc}$														
Variation 3	$-\delta G_c$	$-\delta\eta_c$	$-\delta G_t$	$-\delta\eta_t$	$-\delta G_{pt}$	$-\delta\eta_{pt}$	$-\delta\sigma_{cc}$	$-\delta\eta_{cc}$	$-\delta\sigma_{in}$	$+\delta G_t$	$+\delta G_{pt}$	$+\delta\sigma_{cc}$						
Variation 4	$-\delta G_c$ $-\delta\eta_c$	$-\delta G_t$ $-\delta\eta_t$	$-\delta G_{pt}$ $-\delta\eta_{pt}$	$-\delta\sigma_{cc}$ $-\delta\eta_{cc}$	$+\delta G_t$ $-\delta\eta_t$	$+\delta G_{pt}$ $-\delta\eta_{pt}$	$+\delta\sigma_{cc}$ $-\delta\eta_{cc}$											
Variation 5	$\pm\delta P_c$	$\pm\delta P_t$	$\pm\delta T_c$	$\pm\delta T_t$	$\pm\delta T_{pt}$	$\pm\delta G_f$												
Variation 6	$-\delta G_c$	$-\delta\eta_c$	$-\delta G_t$	$-\delta\eta_t$	$-\delta G_{pt}$	$-\delta\eta_{pt}$	$-\delta\sigma_{cc}$	$-\delta\eta_{cc}$	$-\delta\sigma_{in}$	$+\delta G_t$	$+\delta G_{pt}$	$+\delta\sigma_{cc}$	$\pm\delta P_c$	$\pm\delta P_t$	$\pm\delta T_c$	$\pm\delta T_t$	$\pm\delta T_{pt}$	$\pm\delta G_f$
Variation 7	$-\delta G_c$ - $\delta\eta_c$	$-\delta G_t$ $-\delta\eta_t$	$-\delta G_{pt}$ $-\delta\eta_{pt}$	$-\delta\sigma_{cc}$ $-\delta\eta_{cc}$	$+\delta G_t$ $-\delta\eta_t$	$+\delta G_{pt}$ - $\delta\eta_{pt}$	$+\delta\sigma_{cc}$ $-\delta\eta_{cc}$	$\pm\delta P_c$	$\pm\delta P_t$	$\pm\delta T_c$	$\pm\delta T_t$	$\pm\delta T_{pt}$	$\pm\delta G_f$					
Variation 8	$\pm\delta P_c$	$\pm\delta P_t$	$\pm\delta T_c$	$\pm\delta T_t$	$\pm\delta T_{pt}$	$\pm\delta G_f$	$\pm\delta P_{in}$	$\pm\delta T_{in}$	$\pm\delta n_{hp}$									
Variation 9	$-\delta G_c$ - $\delta\eta_c$	$\pm\delta G_t$ $-\delta\eta_t$	$\pm\delta G_{pt}$ $-\delta\eta_{pt}$	$\pm\delta\sigma_{cc}$ $-\delta\eta_{cc}$														
Variation 10	$-\delta G_c$	$-\delta\eta_c$	$-\delta\eta_t$	$-\delta\eta_{pt}$	$-\delta\eta_{cc}$	$-\delta\sigma_{in}$	$\pm\delta G_t$	$\pm\delta G_{pt}$	$\pm\delta\sigma_{cc}$									
Variation 11	$-\delta G_c$ - $\delta\eta_c$ $\pm\delta G_t$ $-\delta\eta_t$	$-\delta G_c$ $-\delta\eta_c$ $\pm\delta G_{pt}$ $-\delta\eta_{pt}$	$-\delta G_c$ $-\delta\eta_c$ $\pm\delta\sigma_{cc}$ $-\delta\eta_{cc}$	$\pm\delta G_t$ $-\delta\eta_t$ $\pm\delta G_{pt}$ $-\delta\eta_{pt}$	$\pm\delta G_t$ $-\delta\eta_t$ $\pm\delta\sigma_{cc}$ $-\delta\eta_{cc}$	$\pm\delta G_{pt}$ $-\delta\eta_{pt}$ $\pm\delta\sigma_{cc}$ $-\delta\eta_{cc}$												
Variation 12	$-\delta G_c$ - $\delta\eta_c$ $-\delta G_t$ $-\delta\eta_t$	$-\delta G_c$ $-\delta\eta_c$ $-\delta G_{pt}$ $-\delta\eta_{pt}$	$-\delta G_c$ $-\delta\eta_c$ $-\delta\sigma_{cc}$ $-\delta\eta_{cc}$	$-\delta G_t$ $-\delta\eta_t$ $-\delta G_{pt}$ $-\delta\eta_{pt}$	$-\delta G_t$ $-\delta\eta_t$ $-\delta\sigma_{cc}$ $-\delta\eta_{cc}$	$-\delta G_{pt}$ $-\delta\eta_{pt}$ - $\delta\sigma_{cc}$ $-\delta\eta_{cc}$												

6. Boundaries for multiple fault classes

When multiple faults are simulated by summing the influence of each fault parameter, there is the risk that the simulated fault exceeds a severity limit of real faults. In Fig.3, a multiple class D_1 created by two fault parameters is illustrated. The point "0" corresponds here to an engine normal state. Each of the vectors OL_1 and OL_2 results from the change of one fault parameter. Points L_1 and L_2 and vector lengths l_1 and l_2 correspond to an engine health limit. An area Ω_1 of deviation vectors $\vec{Z}$ without errors presents a parallelogram and area Ω_1^* corresponds to deviation vectors $\vec{Z}^*$ with errors. It can be seen that vectors $\vec{Z}$ in the upper right corner of the parallelogram can be longer than base vectors OL_1

and OL_2 produced by a maximal change of the corresponding fault parameters. In other words, simulated faults can have higher severity than real ones.

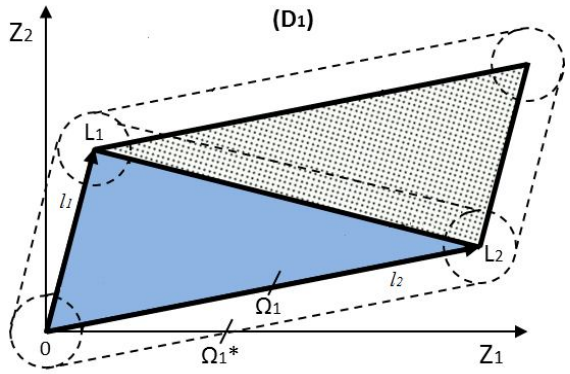

Fig. 5. Straight line boundary

To make the simulated faults more realistic, we previously used a linear boundary L_1L_2 that restricts fault pattern vectors inside the triangle OL_1L_2. However, this boundary becomes too restrictive when the angle L_1OL_2 increases.

An ideal boundary seems to us like a smooth curve formed by a vector that turns from OL_1 to OL_2 and gradually changes its length from l_1 to l_2 proportionally to the turning angle. It is proposed to express this length by:

$$l = l_1 + (l_2 - l_1)\frac{\alpha}{\alpha_{12}}, \qquad (9)$$

where α_i is the angle between a current vector and the first base vector and α_{12} is the angle between the two base vectors. As can be seen, the boundary determined by (9) corresponds to the Archimedean spiral. Figure 6 illustrates action of the proposed boundary: the deviation vectors $\vec{Z}$ that are inside the curve are only accepted.

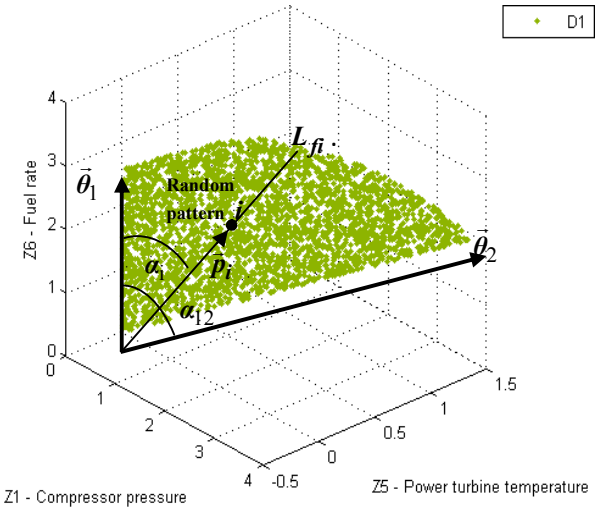

Fig. 6. Archimedeaspiral boundary
(Two fault parameters)

The described boundary rule can be easily extended on the case of three fault parameters illustrated by Fig.7. The boundary vector of the length l determined in the plane of the first and second fault parameters (orange area) is considered as a base vector. The second base vector OL_3 is produced by the third fault parameters. The boundary is determined in the plane of these two base vectors (green area). For the case of four and more fault parameters, we only need to repeat the above procedure.

To better understand the importance of the new boundary, three boundary options have been examined: no boundary (parallelogram area Ω_1), straight line (triangle area Ω_1), and Archimedean spiral. The boundaries were applied for multiple faults of classification variations 2 and 12. For each option and each variation, the three selected neural networks were used by turn for computing average true diagnosis probabilities P_{av}. Table 6 contains all the results, which help to draw the following conclusions. First, the new boundary results in a visible change of the probability P_{av} (up to 0.04). This change can be greater for particular fault classes. Second, for all cases the "Archimedean spiral" probability occupies an intermediate position between "No boundary" probability and "Straight line" probability. This is naturally explained by the fact that the Archimedean spiral curve is situated between the straight line and the parallelogram sides. Third, for the new boundary, the difference between the recognition techniques (three networks) remains small: 0.0045 for classification variation 2 and 0.0133 for variation 12.

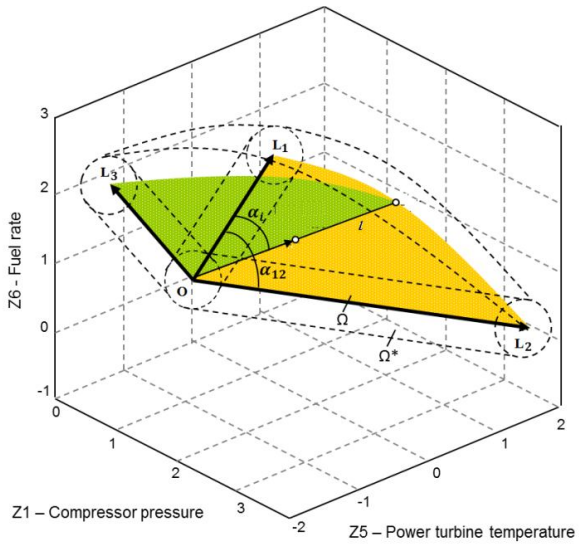

Fig. 7. Archimedean spiral boundary
(Three fault parameters)

Table 5

Average true diagnosis probabilities P_{av} for different classification variations

Variation	Probabilities				Time		
	MLP	RBN	PNN		MLP	RBN	PNN
1	0.8172	0.8169	0.8099		20 min	4 h 11 min	27 min
2	0.8732	0.8759	0.8720		36 min	57 min	6 min
3	0.8091	0.8072	0.8037		59 min	3 h 48 min	29 min
4	0.8490	0.8524	0.8474		5 h 32 min	2 h 44 min	23 min
5	0.8033	0.8080	0.8036		2 h 21 min	2 h 2 min	14 min
6	0.6805	0.7319	0.7316		6 h 42 min	4 h 34 min	36 min
7	0.7362	0.7616	0.7567		5 h 28 min	4 h 41 min	30 min
8	0.7828	0.7965	0.7910		1 h 10 min	3 h 40 min	27 min
9	0.9279	0.9280	0.9260		26 min	1 h 6 min	6 min
10	0.7909	0.8017	0.7930		4 h 39 min	3 h 41 min	22 min
11	0.8075	0.7867	0.7775		4 h 44 min	2 h 21 min	14 min
12	0.8209	0.8184	0.8076		6 h 21 min	2 h 19 min	17 min

Table 6

Average true diagnosis probabilities P_{av} for different fault severity boundaries

Boundary option	Probabilities						
	Variation 2				Variation 12		
	MLP	RBN	PNN		MLP	RBN	PNN
No boundary	0.9164	0.9182	0.9140		0.8288	0.8248	0.8156
Straight line	0.8732	0.8759	0.8720		0.8120	0.8105	0.8005
Archimedean spiral	0.9121	0.9136	0.9091		0.8209	0.8184	0.8076

Conclusions

In investigations and practice of gas turbine diagnosis, fault classifications vary considerably. That is why, the present paper proposes a flexible fault classification that allows creating any necessary totality of fault classes of different types. Twelve classification variations were introduced and investigated in the paper. For each variation, an average probability of correct fault diagnosis was determined using by turn on of three neural networks as a fault recognition technique. Additionally, a new boundary that restricts fault severity was proposed and examined. The following conclusions have been drawn as a result of the investigations:

- the procedure of flexible classification has proven to create any necessary totality of fault classes of different type y complexity. Formation of a new classification variation and change from one variation to another is simple and does not need reprogramming the software;

- for all classification variation examined, three networks provide practically equal average probability of correct diagnosis. This confirms the conclusion made in previous studies that many recognition techniques can have the same diagnostic accuracy;

- among the three networks, the probabilistic neural network seems to be simplest gas turbine fault recognition technique;

- the new boundary (Archimedean spiral) proposed for restricting the severity of simulated faults makes the simulation more realistic and allows to determine more precisely the level of diagnostic accuracy.

Acknowledgments

The work has been carried out with the support of the National Polytechnic Institute of Mexico (research project 20144199) and the National Council of Science and Technology (CONACYT).

References

1. Romessis, C. Bayesian Network Approach for Gas Path Fault Diagnosis [Text] / C. Romessis, K. Mathioudakis // ASME Journal of Engineering for Gas Turbines and Power. − 2006. − Vol. 128, Issue 1. − P. 64-72.

2. Loboda, I. Gas Turbine Fault Recognition Trustworthiness [Text] / I. Loboda, S. Yepifanov // Cientifica, Revista del Instituto Politecnico Nacional de Mexico. − 2006. − Vol. 10, Is. 2. − P. 65-74.

3. Butler, S. An Assessment Methodology for Data-Driven and Model Based Techniques for Engine Health Monitoring [Text] / S. W. Butler, K. R. Pattipati, A. J. Volponi // Proc. IGTI/ASME Turbo Expo 2006, Barcelona, Spain, May 8-11, 2006. − 9 p.

4. García Díaz, J. Diagnóstico de Turbinas de Gas con el Criterio de la Densidad de Probabilidad [Text] / J. García Díaz, I. Loboda, J. L. Pérez Ruiz // Proceedings of the VII International Congress of Electromechanical and Systems Engineering, Mexico City, Mexico, Oct 27-31, 2014. – 7 p.

5. Loboda, I. A Generalized Fault Classification for Gas Turbine Diagnostics on Steady States and Transients [Text] / I. Loboda, S. Yepifanov, Ya. Feldshteyn // Journal of Engineering for Gas Turbines and Power. – 2007. – Vol. 129, No.4. – P. 977-985.

6. Pinelli, M. Gas Turbine Field Performance Determination: Sources of Uncertainties [Text] / M. Pinelli, P. R. Spina // Journal of Engineering for Gas Turbines and Power. – 2002. – Vol. 124, No. 1. – P. 155-160.

7. Pérez Ruiz, J.L. Clasificación Flexible de Fallas para el Diagnóstico Paramétrico de Turbinas de Gas [Text] / J. L. Pérez Ruiz, I. Loboda, I. González Castillo // Proceedings of the VII International Congress of Electromechanical and Systems Engineering, Mexico City, Mexico, Oct 27-31, 2014. – 8 p.

8. Kamboukos, Ph. Comparison of Linear and Nonlinear Gas Turbine Performance Diagnostics [Text] / Ph. Kamboukos, K. Mathioudakis // Journal of Engineering for Gas Turbines and Power. – 2005. – Vol. 127, No. 1. – P. 49-56.

9. Loboda, I. Gas turbine fault recognition using probability density estimation [Text] / I. Loboda // Proceedings of the ASME Turbo Expo 2014 International Technical Congress, Dusseldorf, Germany, June 16-20, 2014. – 13 p., ASME Paper No. GT2014-27265.

Поступила в редакцию 7.11.2014, рассмотрена на редколлегии 19.11.2014

Рецензент: канд. техн. наук, профессор кафедры конструкции авиадвигателей Ю. А. Гусев, Национальный аэрокосмический университет им. Н.Е. Жуковского «Харьковский авиационный институт», Харьков.

ГНУЧКА КЛАСИФІКАЦІЯ ДЕФЕКТІВ ДЛЯ ДІАГНОСТУВАННЯ ГТД

Х. Л. Перес Руіс, І. І. Лобода

Діагностичні алгоритми, які засновано на вимірюваних параметрах і моделях проточної частини, здатні діагностувати не тільки дефекти самої проточної частини, а й несправності систем вимірювання та керування. Так як різноманітність проявів дефектів ГТД велике, вони об'єднуються у обмежене число класів дефектів. Існують різні принципи формування класів та багато конкретних класифікацій, застосовуваних на практиці. На стадії досліджень важко передбачити яка саме класифікація буде потім прийнята в реальній системі контролю, тому дослідники зазвичай експериментують з різними типами класів та їх кількістю. В даній статті пропонується підхід, який дозволяє створення численних варіантів класифікації, що включають складні і більш реалістичні класи дефектів. Цей підхід також дозволяє легку зміну аналізованого варіанта класифікації та методу розпізнавання, застосовуваного для цього варіанту. Для кожної класифікації і кожного методу визначається ймовірність правильного діагностування і час розрахунку, які є критеріями ефективності діагностування. Таким чином, пропонований підхід дозволяє вивчити вплив класифікації дефектів на ефективність діагностування ГТД. Дослідження в статті виконано для силової установки, використовуваної для перекачки природного газу. Проаналізовано 12 варіантів класифікації з використанням трьох методів розпізнавання: Багатошаровий Персептрон, Мережа з Радіальними Засадничими Функціями і Імовірнісна Нейронна Мережа. Крім того, запропоновано нову межу розвитку дефектів. Вона досліджена шляхом порівняння з двома іншими варіантами кордону.

Ключові слова: діагностика ГТД, розпізнавання образів, гнучка класифікація дефектів, кордон розвитку дефектів.

ГИБКАЯ КЛАССИФИКАЦИЯ ДЕФЕКТОВ ДЛЯ ДИАГНОСТИРОВАНИЯ ГТД

Х. Л. Перес Руис, И. И. Лобода

Диагностические алгоритмы, основанные на измеряемых параметрах и моделях проточной части, способны диагностировать не только дефекты самой проточной части, но и неисправности систем измерения и управления. Так как разнообразие проявления дефектов ГТД велико, они объединяются в ограниченное число классов дефектов. Существуют различные принципы формирования классов и много конкретных классификаций, применяемых на практике. На стадии исследований трудно предсказать какая именно классификация будет потом принята в реальной системе контроля, поэтому исследователи обычно экспериментируют с разными типами классов и их количеством. В данной статье предлагается подход, который позволяет создание многочисленных вариантов классификации, включающих сложные и более реалисичные классы дефектов. Этот подход также позволяет легкую смену анализируемого варианта классификации и метода распознавания, применяемого для этого варианта. Для каждой классификации и каждого метода определяется вероятность правильного диагностирования и время расчета, которые являются критериями эффективности диагностирования. Таким образом, предлагаемый подход позволяет изучить влияние классификации дефектов на эффективность диагностирования ГТД. Исследования в статье выполнены для силовой установки, используемой для перекачки природного газа. Проанализировано 12 вариантов классификации с использованием трех методов распознавания: Многослойный Персептрон, Сеть с Радиальными Базисными Функциями и Вероятностная Нейронная Сеть. Кроме того, предложена новая граница развития дефектов. Она исследована путем сравнения с двумя другими вариантами границы.

Ключевые слова: диагностика ГТД, распознавание образов, гибкая классификация дефектов, граница развития дефектов.

Хуан Луис Перес Руис – студент магистратуры, Национальный политехнический институт, Мексика.

Лобода Игорь Игоревич – канд. техн. наук, доцент, преподаватель, Национальный политехнический институт, Мексика, Мехико, e-mail: iloboda@ipn.mx.